NANO LETTERS

Letter

pubs.acs.org/NanoLett

Synthesis and Thermoelectric Properties of Compositional-Modulated Lead Telluride–Bismuth Telluride Nanowire Heterostructures

Haiyu Fang,[†] Tianli Feng,[‡] Haoran Yang,[†] Xiulin Ruan,[‡] and Yue Wu*,[†]

[†]School of Chemical Engineering and [‡]School of Mechanical Engineering, Purdue University, West Lafayette, Indiana 47907, United States

ABSTRACT: We demonstrate the rational solution-phase synthesis of compositional modulated telluride nanowire heterostructures containing lead telluride (PbTe) and bismuth telluride (Bi_2Te_3). By tuning the ratio between PbTe and Bi_2Te_3 through adjusting the amount of critical reactants and precursors during the synthesis, the influence of composition on the thermoelectric properties of the nanowire heterostructures has been investigated in hot pressed nanocomposite pellets. Measurements of the thermoelectric properties show strongly reduced thermal conductivity that leads to an enhanced thermoelectric figure of merit (ZT) of 1.2 at 620 K.

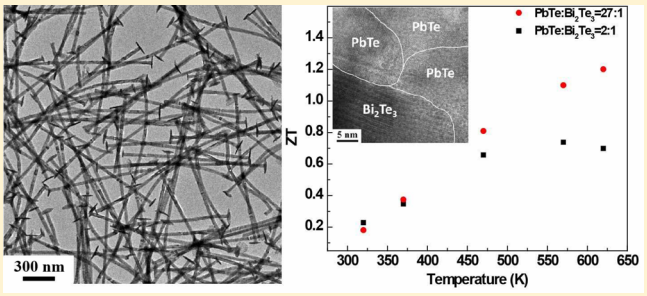

KEYWORDS: *Thermoelectric, nanowire, heterostructure, lead telluride, bismuth telluride*

Recent demands on energy conservation have created a significant interest in thermoelectric materials that can perform a direct conversion between thermal energy and electrical energy for waste heat recovery[1,2] and solid-state cooling[3,4] with improved stability and reliability.[5] The thermoelectric device efficiency is determined by the figure of merit ($ZT = TS^2\sigma/k$). The three factors, Seebeck coefficient (S), electric conductivity (σ), and thermal conductivity (k), are inherently correlated, thus greatly restricting the improvement of ZT.[6] In the past two decades, nanomaterials have been theoretically and experimentally proven to be able to partially decouple the three factors through the unique material properties at nanoscale, such as low energy electron filtering[7−9] and phonon scattering.[10,11] Especially in the most recent literatures, dual-phase nanocomposites were studied intensively because of the extremely low thermal conductivity and great potential for enhancing thermoelectric properties.[12−14] Herein, we use the Te–Bi_2Te_3 barbell nanowire heterostructures developed by our group previously[15] to synthesize PbTe/Bi_2Te_3 "barbell" nanowire heterostructures by converting Te sections into PbTe. The influence of composition (ratio between PbTe and Bi_2Te_3) has been investigated in hot pressed nanocomposite pellets and an enhanced ZT of 1.2 has been achieved at 620 K.

We focus our research on telluride-based thermoelectric materials because of their outstanding figure of merit.[16,17] However, few investigations have been performed on the PbTe/Bi_2Te_3 system. In the existing papers discussing PbTe/Bi_2Te_3 related systems, other elements, such as Sn and Sb, were introduced to form ternary alloy compounds; in other cases, Pb^{2+} or Bi^{3+} were simply used as dopants in Bi_2Te_3 or PbTe, respectively, without the coexistence of both phases.[18−20] Meanwhile, most of these materials were synthesized by high-temperature solid-state reaction, such as zone melting and the Bridgman method,[21,22] which are extremely energy intensive. Moreover, ball milling has been used to obtain nano/micrometer-size grains,[23,24] but this could not only introduce unwanted impurities but also offer little control on the dimensions and uniformity of the grain sizes of each component.

Our synthetic approach to produce PbTe/Bi_2Te_3 nanowire heterostructures involves a three-step solution-phase reaction at a much lower temperature compared to solid-state reactions. The reaction starts with the synthesis of Te nanowires, followed by the growth of Bi_2Te_3 nanoplates on the Te nanowire bodies, and then ends with the conversion of Te sections in the Te–Bi_2Te_3 nanowire heterostructures into PbTe. The synthesis of PbTe–Bi_2Te_3 barbell nanowire heterostructures is carried out in a standard Schlenk line with nitrogen protection. Tellurium dioxide (TeO_2, 99%+), ethylene glycol (EG, 99%+), potassium hydroxide flakes (KOH, 90%), polyvinylpyrrolidone (PVP, average molecule weight 40 000), hydrazine hydrate solution ($N_2H_4{\cdot}H_2O$, 80%), anhydrous hydrazine (98%), bismuth nitrate pentahydrate ($Bi(NO_3)_3{\cdot}5H_2O$, 98%), and lead acetate trihydrate ($Pb(CH_3CO_2)_2{\cdot}3H_2O$, 99%+) were all purchased from Sigma-Aldrich. All of the chemicals are used as received without further purification. In a typical process, 1.5 mmol of TeO_2, 10 mmol of KOH, 0.3 g of PVP, and 15 mL of EG are added into a 50 mL three-neck flask. Nitrogen is purged through the system to keep the reaction in an oxygen-free

Received: January 25, 2013
Revised: April 10, 2013
Published: April 10, 2013

   dx.doi.org/10.1021/nl400319u | *Nano Lett.* 2013, 13, 2058–2063

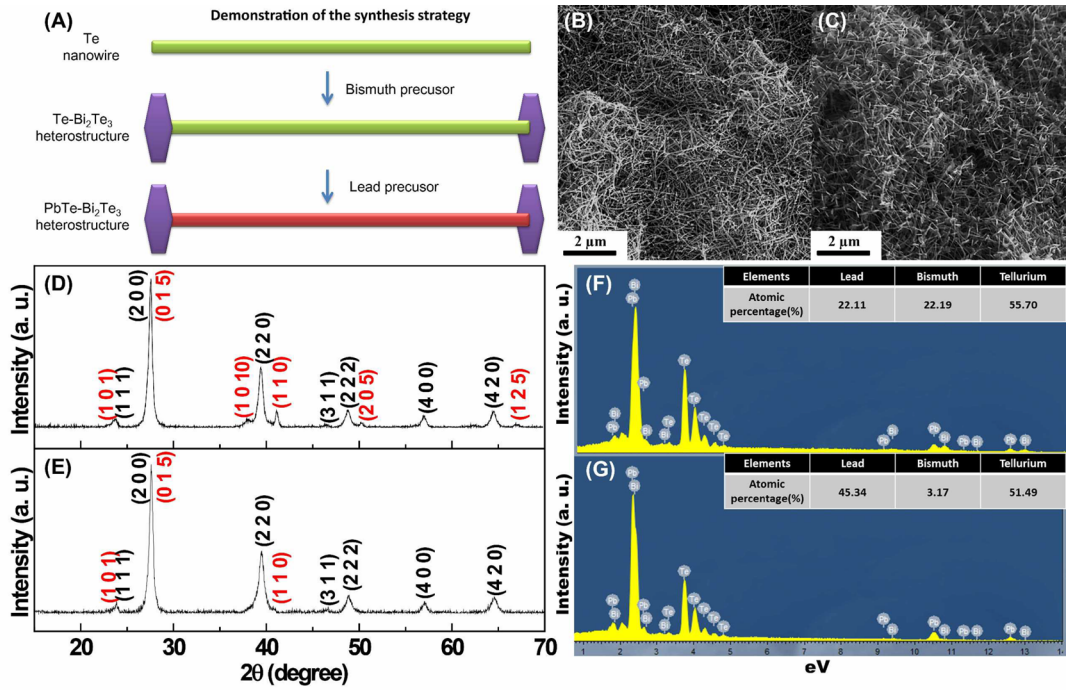

Figure 1. (A) Scheme of the transformation in the three-step synthesis of PbTe–Bi_2Te_3 barbell nanowire heterostructures. SEM images of the nanowire heterostructures with composition ratio of (B) PbTe/Bi_2Te_3 = 27:1 and (C) PbTe/Bi_2Te_3 = 2:1. XRD patterns of (D) PbTe/Bi_2Te_3 = 2:1 sample and (E) PbTe/Bi_2Te_3 = 27:1 sample. The black text refers to PbTe and the red text refers to Bi_2Te_3. Energy dispersive X-ray spectroscopy (EDS) of (F) PbTe/Bi_2Te_3 = 2:1 sample and (G) PbTe/Bi_2Te_3 = 27:1 sample. Inlaid tables give the atomic percentage of Pb, Bi, and Te.

environment. The mixture is stirred and heated to 140 °C. After all of the chemicals are dissolved thoroughly, 0.20 mL of 80% hydrazine hydrate solution is injected into the reaction, and the yellow-transparent solution becomes a black slurry, which is kept at 140 °C for 1 h to allow Te nanowires to form completely. Meanwhile, 0.6 mmol (for PbTe/Bi_2Te_3 = 2:1, molar ratio) or 0.1 mmol (for PbTe/Bi_2Te_3 = 27:1, molar ratio) of $Bi(NO_3)_3{\cdot}5H_2O$ are added into 5 mL of EG in a glass vial to form a solution that is kept at 100–120 °C. After that, the temperature of Te nanowire solution is raised to 160 °C, and the $Bi(NO_3)_3{\cdot}5H_2O$/EG solution is hot-injected into the flask. The reaction continues at 160 °C for another hour. At the same time, 0.6 mmol (for PbTe/Bi_2Te_3 = 2:1) or 1.35 mmol (for PbTe/Bi_2Te_3 = 27:1) of $Pb(CH_3CO_2)_2{\cdot}3H_2O$ are added into 5 mL of EG in a glass vial to form a solution which is kept at 100–120 °C. After 1 h, 0.4 mL of anhydrous hydrazine is first added into the reaction and then the $Pb(CH_3CO_2)_2{\cdot}3H_2O$/EG solution is injected into the reaction, which continues for another 1 h before naturally cooling down to room temperature. The as-obtained product is centrifuged followed by washing with deionized water three times and ethanol twice. The whole procedure is shown in Figure 1A.

The products of the PbTe/Bi_2Te_3 barbell nanowire heterostructures with different compositions are first characterized by scanning electron microscopy (SEM) (Figure 1B,C), X-ray diffraction (XRD) (Figure 1D,E), and energy dispersive X-ray spectroscopy (EDS) (Figure 1F,G). Interestingly, both products show nanowire shape observed from SEM studies and both XRD spectra can be readily indexed into PbTe (JCPDS No. 38-1435) and Bi_2Te_3 (JCPDS No. 15-0863) without Te impurity peaks, proving a complete conversion of Te into PbTe. However, the intensity of the Bi_2Te_3 peaks in the XRD patterns is slightly different. Bi_2Te_3 peaks in the PbTe/Bi_2Te_3 = 27:1 sample spectrum (Figure 1E) are almost unidentifiable because of the low Bi_2Te_3 concentration. Meanwhile, the (1 1 0) peak of Bi_2Te_3 grows much higher and those peaks not appearing in the PbTe/Bi_2Te_3 = 27:1 sample spectrum, such as (2 0 5) and (1 2 5), start to arise in the PbTe/Bi_2Te_3 = 2:1 sample spectrum (Figure 1D), which clearly indicates an increased amount of Bi_2Te_3 phase. Furthermore, the composition difference between the two samples is further confirmed by EDS (Figure 1F,G), which shows that the elements in both samples have stoichiometric ratios with nearly negligible Te redundancy (0.14% for the PbTe/Bi_2Te_3 = 2:1 sample and 0.69% for the PbTe/Bi_2Te_3 = 27:1 sample). The Bi_2Te_3 molar percentage of 33.4% in the PbTe/Bi_2Te_3 = 2:1 sample (theoretical value: 33.3%) and of 3.38% in the PbTe/Bi_2Te_3 = 27:1 sample (theoretical value: 3.57%) were obtained, which proves that our strategy to control over the molar ratio between PbTe and Bi_2Te_3 during the synthesis by adjusting the amount of the initial precursors is quite successful. Notably, these two compositions represent the boundary of a wide tunable range where we can vary the ratio between PbTe and Bi_2Te_3 while still maintaining the nanowire heterostructures; if the PbTe/Bi_2Te_3 ratio is smaller than 2:1, the extra Bi precursor would lead to the random deposition of Bi_2Te_3 on the nanowire body and suppress the selective growth of Bi_2Te_3 plates on the ends of the initial Te nanowires; if the PbTe/Bi_2Te_3 ratio is larger than 27:1, the low concentration of Bi precursor amount would not be enough to form two obvious plates on the two ends of Te nanowire.

The PbTe/Bi_2Te_3 barbell nanowire heterostructures are further studied by transmission electron microscopy (TEM). The low-magnification TEM images of the PbTe/Bi_2Te_3 = 2:1 sample (Figure 2A) and the PbTe/Bi_2Te_3 = 27:1 sample (Figure 2C) clearly display the uniformity of the barbell morphology with smooth surfaces. The statistical analysis on Figure 2A,C shows the similar average diameters of the PbTe

dx.doi.org/10.1021/nl400319u | *Nano Lett.* 2013, 13, 2058–2063

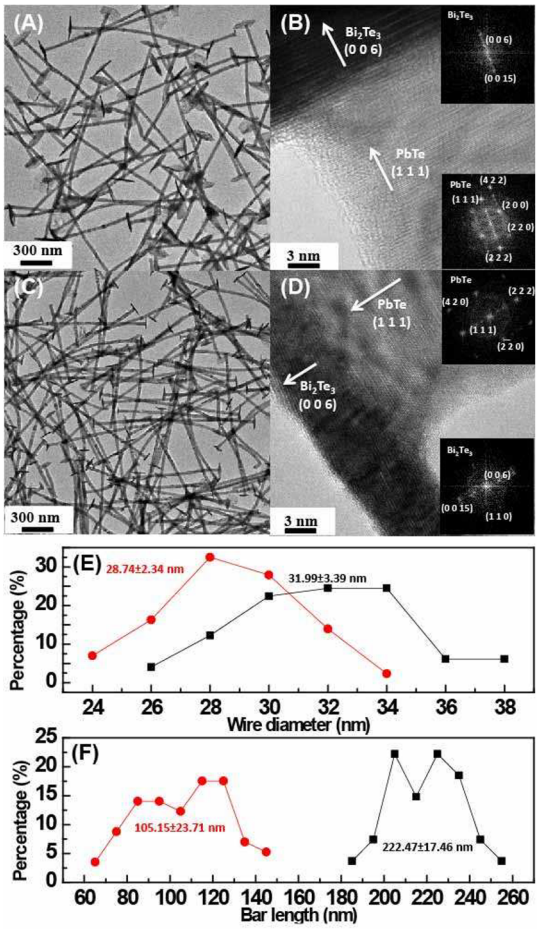

Figure 2. (A,C) Low-magnification TEM images of the PbTe/Bi_2Te_3 barbell nanowire heterostructures with compositions of PbTe/Bi_2Te_3 = 2:1 and PbTe/Bi_2Te_3 = 27:1. (B,D) HRTEM images of the interface between Bi_2Te_3 bar and PbTe nanowire body in the samples with the composition of PbTe/Bi_2Te_3 = 2:1 and PbTe/Bi_2Te_3 = 27:1. (E,(F) The histogram of the diameter of PbTe nanowire body and the length of Bi_2Te_3 bars, respectively. The red curves refer to the sample of PbTe/Bi_2Te_3 = 27:1 and the black curves refer to the sample of PbTe/Bi_2Te_3 = 2:1.

nanowire part (Figure 2E) of 28.74 ± 2.34 nm (for the PbTe/Bi_2Te_3 = 2:1 sample) and 31.99 ± 3.39 nm (for the PbTe/Bi_2Te_3 = 27:1). The average lengths of the Bi_2Te_3 bars (Figure 2F), however, are quite different in the two samples with of 222.47 ± 17.46 nm in the PbTe/Bi_2Te_3 = 2:1 sample and 105.15 ± 23.71 nm in the PbTe/Bi_2Te_3 = 27:1 sample. Such a big difference (~120 nm) is consistent with the disparity of Bi molar concentration in the two samples. Moreover, the high-resolution TEM (HRTEM) images taken at the interface of the PbTe nanowires and Bi_2Te_3 bars (Figure 2C,D) reveal several important points: first, the nearly defects-free lattices infer the single crystalline nature of both the nanowire and bar parts; second, the fast Fourier transform (FFT) performed individually on the nanowire and bar parts show the pure PbTe and Bi_2Te_3 phases, respectively; third, the axial direction of PbTe and Bi_2Te_3 is perpendicular to the (1 1 1) and (0 0 6) crystal planes, respectively. There is a 4.01% lattice mismatch at the PbTe/Bi_2Te_3 interface, which is larger than the Te/Bi_2Te_3 interface lattice mismatch (1.62%) but still small enough to tolerate epitaxial growth.

The rational and reproducible PbTe-Bi_2Te_3 barbell nanowire heterostructures synthesis procedure confirmed by various characterization methods provides us the opportunity to further investigate their bulk thermoelectric properties through mass production. The as-synthesized products are washed with hydrazine to remove the capping ligands on the surfaces of barbell nanowire heterostructures and vacuum-dried at room temperature following the detailed procedures described in our previous paper.[15] Afterward, the cleaned and dried nanowire powder is hot-pressed at 150 °C and 165 MPa for half an hour and then naturally cooled down to room temperature while the pressure is maintained at 165 MPa. A subsequent annealing at 300 °C for two hours is followed to eliminate unwanted defects created during the hot press and remove retained capping ligands. Digital photos (insets, Figure 3A,B) of the two samples

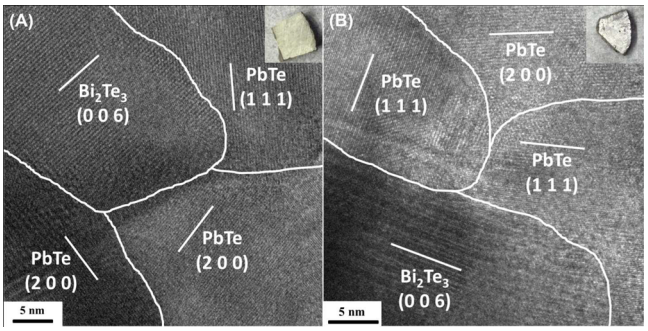

Figure 3. (A,B) Cross section HRTEM images of the sample PbTe/Bi_2Te_3 = 2:1 and the sample PbTe/Bi_2Te_3 = 27:1 pellets, which clearly show nanoscale PbTe and Bi_2Te_3 crystal domains and preserved grain boundaries inside the nanocomposites. The insets are digital photos of two PbTe-Bi_2Te_3 pellets after hot pressing and subsequent annealing.

show a slight color variation because of the different compositions. The temperatures for hot pressing and annealing are much lower compared to the alloying temperature shown in the equilibrium diagram of the PbTe and Bi_2Te_3 binary system and the possible ternary compounds ($PbBi_xTe_y$), such as $PbBi_2Te_4$, $PbBi_4Te_7$, or $Pb_3Bi_4Te_9$ can only form at 850 K.[25,26] The preservation of the compositions (PbTe and Bi_2Te_3 instead of their alloys) and nanoscale grain boundaries are clearly demonstrated by the HRTEM studies performed on the cross sections of the hot-pressed/annealed samples of PbTe/Bi_2Te_3 = 2:1 (Figure 3A) and PbTe/Bi_2Te_3 = 27:1 (Figure 3B) in both of which the different nanoscale grains can be readily identified as PbTe and Bi_2Te_3 phases with random orientations.

After the fabrication process, the pellets are micromachined and polished into regular rectangular shape with identical size before the measurement of electrical conductivity, Seebeck coefficient and thermal conductivity (Figure 4, the black square curves and red dot curves are obtained from the PbTe/Bi_2Te_3 = 2:1 sample and PbTe/Bi_2Te_3 = 27:1 sample, respectively). The electrical conductivity is measured through a standard four-probe method with a maximum temperature fluctuation of ±2 K. The Seebeck coefficient is measured by bridging the sample between a heater and heat sink and testing the voltage difference between the hot and the cold sides with a maximum temperature fluctuation of ±0.2 K and a voltage resolution of 50 nV. The thermal conductivity (k) is measured through thermal diffusivity (α) and specific heat (C_p) and then calculated via the equation $\kappa = \alpha\rho C_p$ (ρ is the density). In the temperature range from 310 to 650 K, the electric

dx.doi.org/10.1021/nl400319u | Nano Lett. 2013, 13, 2058−2063

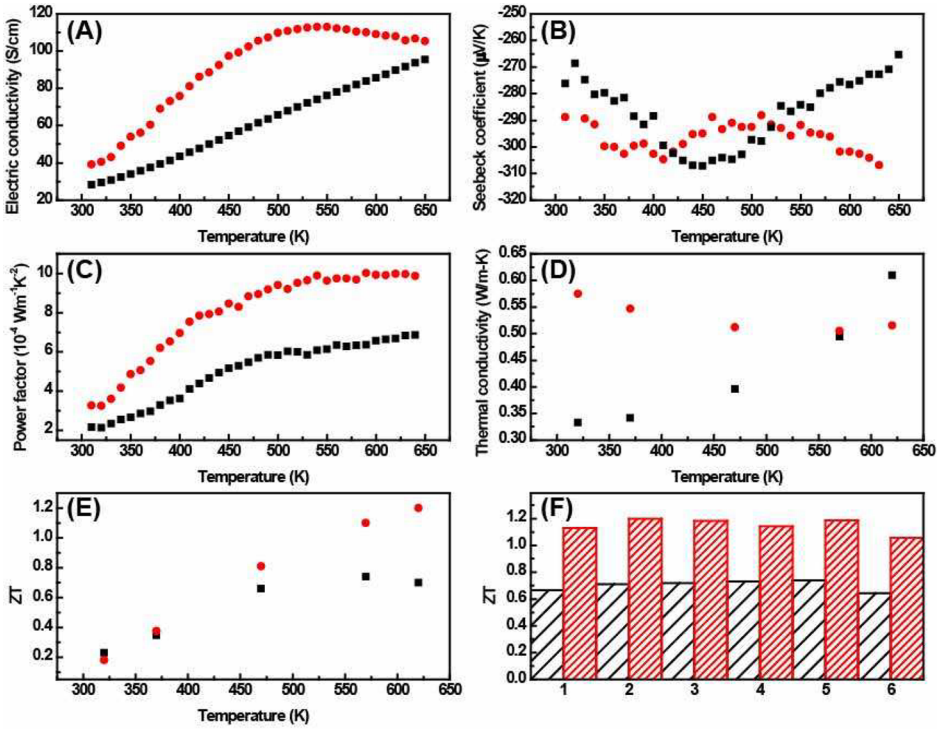

Figure 4. Thermoelectric properties of the $PbTe/Bi_2Te_3$ = 2:1 sample and the $PbTe/Bi_2Te_3$ = 27:1 sample made by hot pressing and subsequently annealing the heterostructures. The red dot curves and the red bars stand for the $PbTe/Bi_2Te_3$ = 27:1 sample and the black square curves and the black bars stand for the $PbTe/Bi_2Te_3$ = 2:1 sample. (A) Electrical conductivity, (B) Seebeck coefficient, (C) power factor, (D) thermal conductivity, (E) ZT of a typical sample measured between 300 and 650 K, and (F) the distribution of peak ZT values based on the different Seebeck coefficients measured on six samples from each composition.

conductivity of the $PbTe/Bi_2Te_3$ = 2:1 sample increases from 28 to 90 S/cm, while the $PbTe/Bi_2Te_3$ = 27:1 sample has a higher electric conductivity that increases from 39 to 113 S/cm at 550 K and then decreases to 105 S/cm (Figure 4A). The different conductivities could be explained in two aspects: first, a larger Bi_2Te_3 composition could lead to more $PbTe/Bi_2Te_3$ interfaces, which could scatter the electron transport; second, even though the same process was applied to fabricate the two pellets, the relative density of $PbTe/Bi_2Te_3$ = 27:1 pellet (76.27%) is higher than that of $PbTe/Bi_2Te_3$ = 2:1 pellet (68.22%). In fact, because of the noticeable porosity in both pellets, the electric conductivities of both samples are much smaller compared to those of bulk Bi_2Te_3 (880 S/cm)[23] and PbTe (526 S/cm).[17] However, our samples' electric conductivities are still comparable to other PbTe-based nanocomposites at high-temperature range where the optimum ZT occurs, such as PbTe/BaTe (150 S/cm at 750K)[12] and $PbTe/PbSnS_2$ (140 S/cm at 500K).[13] Both samples with different composition show n-type behavior as shown by the negative Seebeck coefficients observed with absolute value between 250 μV/K and 310 μV/K (Figure 4B), which are slightly improved compared to the bulk Bi_2Te_3 (optimum Seebeck coefficient, 220 μV/K)[23] and the bulk PbTe (optimum Seebeck coefficient, 230 μV/K).[17] The enhanced Seebeck coefficient could partially result from the energy filtering effect at the $PbTe/Bi_2Te_3$ interface with a band offset around 0.8 eV.[27,28] The temperature-dependent behavior of the Seebeck coefficient is related with the bipolar effect in which the thermal excited holes have opposite contribution to Seebeck coefficient thereby reducing the absolute value.[6] Such a bipolar effect becomes more obvious with increasing temperature: in both the $PbTe/Bi_2Te_3$ = 27:1 and the $PbTe/Bi_2Te_3$ = 2:1 samples, the Seebeck coefficients reach to the maximum absolute values between 400 and 450 K and then start to decrease. The only difference between two samples is that in the $PbTe/Bi_2Te_3$ = 27:1 the Seebeck coefficient starts to increase again after 520 K due to the saturation of the electric conductivity while in the $PbTe/Bi_2Te_3$ = 2:1 sample the electrical conductivity keeps increasing (due to enhanced hole transport), thus further decreasing the Seebeck coefficient. The most interesting property of the two samples is the extremely low thermal conductivity (Figure 4D). At temperatures between 310 and 620 K, the thermal conductivity of the $PbTe/Bi_2Te_3$ = 2:1 sample ranges from 0.333 to 0.610 W/m·K which is lower than that of the $PbTe/Bi_2Te_3$ = 27:1 sample (0.575−0.515 W/m·K). The thermal conductivity results highlight a few important points. First, the overall thermal conductivities of both samples are significantly smaller than the lowest thermal conductivity of bulk Bi_2Te_3 (1.4 W/m·K at 345 K)[23] and PbTe (1.4 W/m·K at 720 K),[17] as well as other telluride based nanocomposites, such as PbTe/BaTe (0.9 W/m·K at 750 K)[12] and $PbTe/PbSnS_2$ (0.9 W/m·K at 500 K);[13] second, the calculated lattice thermal conductivities (Lorenz number = 2.44×10^{-8} $W{\cdot}S^{1-}{\cdot}K^{-2}$) of our nanocomposites are from 0.307 to 0.427 W/m·K for the $PbTe/Bi_2Te_3$ = 2:1 sample and from 0.350 to 0.550 W/m·K for the $PbTe/Bi_2Te_3$ = 27:1 sample, respectively. The lattice thermal conductivities of both samples are much smaller than bulk Bi_2Te_3 (0.8 W/m·K at 345 K)[23] and PbTe (0.8 W/m·K at 720 K),[17] as well as PbTe/BaTe (0.63 W/m·K at 750 K)[12] and $PbTe-PbSnS_2$ (0.73 W/m·K at 500 K)[13] nanocomposites. On the basis of the measured electrical conductivities, Seebeck coefficients, and thermal conductivities, we calculate the ZT of the two nanocomposite samples and plot the temperature-dependent curves in Figure 4E. The peak ZT of the $PbTe/$

dx.doi.org/10.1021/nl400319u | Nano Lett. 2013, 13, 2058−2063

Bi_2Te_3 = 2:1 sample is 0.72 at 570 K, which is smaller than the one of the PbTe/Bi_2Te_3 = 27:1 sample (1.20 at 620 K). Notably, the peak ZT value (1.20 at 620 K) of PbTe/Bi_2Te_3 = 27:1 sample is better than that of the bulk Bi_2Te_3 (1.05 at 320 K)[23] and slightly higher than the ZT (1.19) of the state-of-the-art bulk n-type bulk PbTe at the same temperature of 620 K.[17]

We have also performed a statistic study on multiple samples (six samples for each composition). Notably, the electrical conductivity and thermal conductivity of each group of six samples with the same composition are nearly same (within 1−2%), however, the biggest variation comes from the measurement of Seebeck coefficient when these samples are mounted between a heater and a heat sink where every time the thermal interface resistance between the sample and the heater/heat sink will be different, leading to the tiny variation of "effective" temperature difference across the samples and resulting to the distribution of ZT values shown in Figure 4F. But for the same composition, the peak ZT values of the six samples all happen at the same temperature (570 K for the PbTe/Bi_2Te_3 = 2:1 samples and 620 K for the PbTe/Bi_2Te_3 = 27:1 samples), thus shows the uniformity of our materials and sample preparation.

The enhanced ZT values in our nanowire heterostrutures mainly result from the low thermal conductivities observed in both nanocomposites, however, the measured thermal conductivities of the two nanowire heterostructures with different compositions show completely different temperature dependence, for which we have applied a theoretical analysis of our materials. It has been already known that the total thermal conductivity is contributed by lattice k_l, electron k_e, and bipolar effect $k_{e\text{-}h}$[29]

$$k_{total} = k_e + k_l + k_{e-h} \quad (1)$$

The electron part k_e can be estimated by Wiedemann−Franz law $k_e = \sigma(T)L_0T$, $L_0 = 2.44 \times 10^{-8}$ $W{\cdot}S^{-1}{\cdot}K^{-2}$, which is approximately applicable for quasicrystals and approximants[30,31] and has been used in many other works.[29−32] To understand the remaining part $k_{total} - k_e$, we use the effective medium approximation (EMA) and empirical fitting to find the lattice contribution and finally obtain the bipolar effect contribution. First, existence of the porosity[33−35] can decease the lattice thermal conductivity according to $k_l = (1 - P)^{3/2}k_f$, where k_f is the lattice thermal conductivity of the imagined fully dense nanocomposites, $P = 1 - \rho/\rho_f$ is the porosity, whose values are 0.316 and 0.2364 for the 2:1 and 27:1 PbTe/Bi_2Te_3 nanocomposites, respectively. Second, k_f can be described[32,36−38] as $1/k_f = 1/k_0 + 2R_k/d$, where k_0 is the lattice thermal conductivity of the imagined nonboundary-resistance nanocomposite, R_k is the thermal boundary and interfacial resistance (Kapitza resistance), and d is the average grain diameter. The temperature dependence of Kapitza resistance can be expressed as $R_k \sim T^{\beta}$ where the value of β can be either positive[32] or negative.[37] Additionally, k_0 can be evaluated from EMA originally done by Bruggemann[39] and developed by Nan et al.[40−42]

$$k_0 = k_1 \frac{k_2 + (n-1)k_1 - (n-1)p_1(k_1 - k_2)}{k_2 + (n-1)k_1 + p_2(k_1 - k_2)} \quad (2)$$

Where $n = 3/\Psi$ is the shape factor of nanoparticles with sphericity $\Psi \leq 1$, p_2 is the volume fraction of Bi_2Te_3, and k_1 and k_2 are the lattice thermal conductivity[43,44] of bulk PbTe and bulk Bi_2Te_3, respectively. Finally the lattice thermal conductivity can be expressed by

$$k_l = (1 - P)^{3/2}\left(\frac{1}{k_0} + \frac{2R_k}{d}\right)^{-1} \quad (3)$$

Considering that the bipolar contribution increases[45] while the lattice contribution decreases with increasing temperature proven by experiment and simulation,[46,47] we assume that at low temperature the bipolar contribution is negligible compared to the lattice contribution that is estimated as $k_l = k_{total} - k_e$ that can be used to determine the fitting parameters R_k and n. After that we can use eq 3 to predict the high-temperature range lattice thermal conductivity and finally obtain the contribution of the bipolar effect at the high temperature range with the results shown in Figure 5. For the

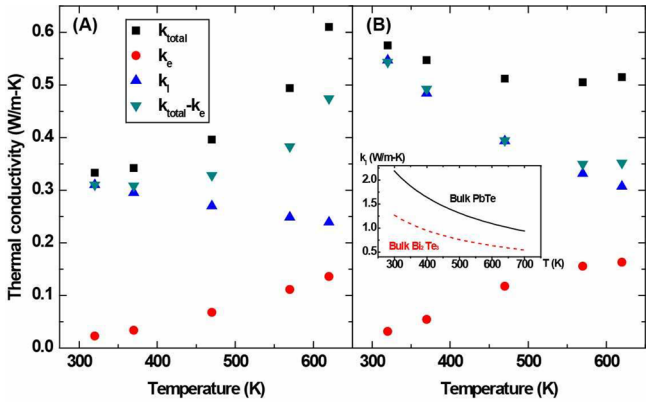

Figure 5. Thermal conductivity of the 2:1 (A) and 27:1 (B) PbTe/Bi_2Te_3 nanocomposites, including the total thermal conductivity (black squares), electron contribution (red circles), and lattice contribution (upward-pointing triangles). The down-triangular denotes the remaining part after subtracting the electron contribution from the total thermal conductivity. The inlaid figure in (B) shows the lattice thermal conductivity of bulk PbTe[44,48] and bulk Bi_2Te_3.[46,47]

PbTe/Bi_2Te_3 = 27:1 sample (Figure 5B), the fitting results shows that the Kapitza resistance increases with temperature with an approximately linear dependence ($\beta \approx 1$), which makes the total thermal conductivity decrease with temperature more quickly than both bulk PbTe and bulk Bi_2Te_3. At temperatures of 300 and 650 K, the values of R_k are approximately 1.04×10^{-8} $m^2{\cdot}K{\cdot}W^{-1}$ and 1.88×10^{-8} $m^2{\cdot}K{\cdot}W^{-1}$ determined by fitting the experimental thermal conductivity data at low temperature, respectively, which are of the same order as the bulk thermal resistance and cannot be neglected, as the phonon mean free path of bulk PbTe and bulk Bi_2Te_3 are of same order as the grain size $d \approx 30$ nm. The total thermal conductivity is mostly contributed by lattice vibration since the PbTe bipolar effect starts at around 600 K. For the PbTe/Bi_2Te_3 = 2:1 sample (Figure 5A) that contains more Bi_2Te_3 in which the bipolar effect becomes relevant at about 350 K, the total thermal conductivity increases dramatically with temperature above 350 K. The Kapitza resistance $R_k = 1.89 \times 10^{-8}$ $m^2{\cdot}K{\cdot}W^{-1}$ at 320 K is higher than that of the PbTe/Bi_2Te_3 = 27:1 sample at the same temperature due to the increased fraction of Bi_2Te_3 that leads to the increased amount of compositional interfaces/grain boundaries. In conclusion, the distinct temperature dependence of the two nanowire heterostructure systems is indeed due to the different compositions, which decides the temperature at which the bipolar effect becomes dominant. More importantly, the well-preserved compositional interfaces/grain boundaries in the

dx.doi.org/10.1021/nl400319u | Nano Lett. 2013, 13, 2058−2063

nanocomposite samples result in the large Kapitza resistance, thus leading to the extremely low thermal conductivity in both samples.

To summarize, we have developed a rational synthesis of PbTe−Bi_2Te_3 "barbell" nanowire heterostructures through a solution-phase one-pot three-step reaction. Through the control of the ratio between PbTe and Bi_2Te_3, the thermoelectric properties can be manipulated to achieve a largely reduced thermal conductivity and enhanced thermoelectric figure of merit (ZT) of 1.2 at 620 K.

AUTHOR INFORMATION

Corresponding Author

*Tel: +1-765-494-6028. E-mail: yuewu@purdue.edu. Fax: +1-765-494-0805.

Notes

The authors declare no competing financial interest.

ACKNOWLEDGMENTS

Y. Wu thanks the support from Air Force Office of Scientific Research (Award Number FA9550-12-1-0061), DuPont Young Faculty Award, and a partial support from NSF/DOE Thermoelectric Partnership (Award Number 1048616). T.L.F. and X.L.R. acknowledge the partial support from National Science Foundation (Award Number CBET-1150948)

REFERENCES

(1) Bell, L. E. *Science* **2008**, *321*, 1457.
(2) *Thermoelectrics Handbook: Macro to Nano*; Rowe, D. M., Eds.; CRC/Taylor& Francis: Boca Raton, FL, 2006.
(3) Mahan, G.; Sales, B. *Phys. Today* **1997**, *50*, 42.
(4) Goldsmid, H. J. *Thermoelectric refrigeration*; Plenum Press: New York, 1964.
(5) DiSalvo, F. J. *Science* **1999**, *285*, 703.
(6) Snyder, G. J.; Toberer, E. S. *Nat. Mater.* **2008**, *7*, 105.
(7) Faleev, S. V.; Leonard, F. *Phys. Rev. B* **2008**, *77*, 214304.
(8) Zebarjadi, M.; Esfarjani, K.; Shakouri, A.; Bahk, J. H.; Bian, Z.; Zeng, G.; Bowers, J.; Lu, H.; Zide, J.; Gossard, A. *Appl. Phys. Lett.* **2009**, *94*, 202105.
(9) Ko, D. K.; Kang, Y. J.; Murry, C. B. *Nano Lett.* **2011**, *11*, 2841.
(10) Poon, S. J.; Limtragool, K. *J. Appl. Phys.* **2011**, *110*, 114306.
(11) Cahill, D. G.; Ford, W. K.; Goodson, K. E.; Mahan, G. D.; Majumdar, A.; Maris, H. J.; Merlin, R.; Phillpot, S. R. *J. Appl. Phys.* **2003**, *93*, 793.
(12) Lo, S. H.; He, J.; Biswas, K.; Kanatzidis, M. G.; Dravid, V. P. *Adv. Funct. Mater.* **2012**, *22*, 5175.
(13) Girard, S. N.; Chasapis, T. C.; He, J.; Zhou, X.; Hatzikraniotis, E.; Uher, C.; Paraskevopoulos, K. M.; Dravid, V. P.; Kanatzidis, M. G. *Energy Environ. Sci.* **2012**, *5*, 8716.
(14) Biswas, K.; He, J.; Blum, I. D.; Wu, C. I.; Hogan, T. P.; Seidman, D. N.; Dravid, V. P.; Kanatzidis, M. G. *Nature* **2012**, *489*, 414.
(15) Zhang, G.; Fang, H.; Yang, H.; Jauregui, L. A.; Chen, P. Y.; Wu, Y. *Nano Lett.* **2012**, *12*, 3627.
(16) Goldsmid, H. J. *Proc. Phys. Soc. London* **1958**, *71*, 633.
(17) LaLonde, A. D.; Pei, Y.; Snyder, J. G. *Energy Environ. Sci.* **2011**, *4*, 2090.
(18) Oh, T. S. *J. Electron. Mater.* **2009**, *38*, 1041.
(19) Su, T.; Zhu, P.; Ma, H.; Ren, G.; Guo, J.; Imai, Y.; Jia, X. *Solid State Commun.* **2006**, *138*, 580.
(20) Zhu, P. W.; Imai, Y.; Isoda, Y.; Shinohara, Y.; Jia, X.; Zou, G. *Mater. Trans.* **2005**, *46*, 761.
(21) Fan, S.; Zhao, J.; Guo, J.; Yan, Q.; Ma, J.; Hng, H. H. *Appl. Phys. Lett.* **2010**, *96*, 182104.
(22) Yamashita, O.; Tomiyoshi, S.; Makita, K. *J. Appl. Phys.* **2003**, *93*, 368.
(23) Poudel, B.; Hao, Q.; Ma, Y.; Lan, Y.; Minnich, A.; Yu, B.; Yan, X.; Wang, D.; Muto, A.; Vashaee, D.; Chen, X.; Liu, J.; Dresselhaus, M. S.; Chen, G.; Ren, R. *Science* **2008**, *320*, 634.
(24) Kuo, C. H.; Hwang, C. S.; Jeng, M. S.; Su, W. S.; Chou, Y. W.; Ku, J. R. *J. Alloys Compd.* **2010**, *496*, 687.
(25) Golovanova, N. S.; Zlomanov, V. P. *Inorg. Mater.* **1983**, *19*, 669.
(26) Hirai, T.; Takeda, Y.; Kurata, K. *J. Less Common Metals* **1967**, *13*, 352.
(27) Green, M.; Lee, M. J.; Miles, R. E. *Surf. Sci.* **1968**, *12*, 403.
(28) Haneman, D. *J. Phys. Chem. Solids* **1959**, *11*, 205.
(29) Takeuchi, T. *Z. Kristallogr.* **2009**, *224*, 35.
(30) Mahan, G. D.; Bartkowiak, M. *Appl. Phys. Lett.* **1999**, *74*, 953.
(31) Macia, E. *Appl. Phys. Lett.* **2002**, *81*, 88.
(32) Toprak, M.; Stiewe, C.; Platzek, D.; Williams, S.; Bertini, L.; Muller, E.; Gatti, C.; Zhang, Y.; Rowe, M.; Muhammed, M. *Adv. Funct. Mater.* **2004**, *14*, 1189.
(33) Bauer, T. H. *Int. J. Heat Mass Transfer* **1993**, *36*, 4181.
(34) Raghavan, S.; Wang, H.; Dinwiddie, R. B.; Porter, W. D.; Mayo, M. J. *Scr. Mater.* **1998**, *39*, 1119.
(35) Yadav, G. G.; Zhang, G.; Qiu, B.; Suspreny, J. A.; Ruan, X.; Wu, Y. *Nanoscale* **2011**, *3*, 4078.
(36) Evans, W.; Prasher, R.; Fish, J.; Meakin, P.; Phelan, P.; Keblinski, P. *Int. J. Heat Mass Transfer* **2008**, *51*, 1431.
(37) Amrit, J. *J. Phys. D: Appl. Phys.* **2006**, *39*, 4472.
(38) Yang, H.; Bai, G. R.; Thompson, L. J.; Eastman, J. A. *Acta Mater.* **2002**, *50*, 2309.
(39) Bruggeman, DAG . *Ann. Phys. (Leipz.)* **1935**, *24*, 636.
(40) Hamilton, R. L.; Crosser, O. K. *Ind. Eng. Chem. Fundam.* **1962**, *1*, 187.
(41) Wang, J.; Yi, X. *Compos. Sci. Technol.* **2004**, *64*, 1623.
(42) Nan, C. W.; Birringer, R.; Clarke, D. R.; Gleiter, H. *J. Appl. Phys.* **1997**, *81*, 6692.
(43) Goldsmid, H. J. *Proc. Phys. Soc. B* **1956**, *69*, 203.
(44) Fedorov, V. I.; Machuev, V. I. *Sov. Phys. Solid State USSR* **1969**, *11*, 1116.
(45) Volklein, F.; Kessler, E. *Phys. Status Solidi B* **1990**, *158*, 521.
(46) Satterthwaite, C. B.; Ure, J. R. W. *Phys. Rev.* **1957**, *108*, 1164.
(47) Huang, B. L.; Kaviany, M. *Phys. Rev. B* **2008**, *77*, 125209.
(48) Qiu, B.; Bao, H.; Zhang, G.; Wu, Y.; Ruan, X. *Comput. Mater. Sci.* **2011**, *53*, 278.